Am J Clin Exp Urol 2019;7(3):153-158
www.ajceu.us /ISSN:2330-1910/AJCEU0097273

Original Article

MRI-based method for lower urinary tract dysfunction in adult male mice

Dalton T McLean[3,4*], David R Rutkowski[1,2*], Teresa Liu[3,5], Diego Hernando[2,5,6], William A Ricke[3,5], Alejandro Roldán-Alzate[1,2,5,7]

[1]Mechanical Engineering, [2]Radiology, [3]Urology, [4]Cancer Biology, [5]George M. O'Brien Center of Research Excellence, [6]Medical Physics, [7]Biomedcial Engineering, University of Wisconsin, Madison, WI, USA. [*]Co-first authors.

Received May 20, 2019; Accepted May 30, 2019; Epub June 15, 2019; Published June 30, 2019

Abstract: Benign prostatic hyperplasia (BPH) develops in the majority of men as they age. As a result, lower urinary tract symptoms (LUTS) often develop, which significantly decrease quality of life. One model of studying BPH/LUTS in mice is to use a hormone-induced model of lower urinary tract dysfunction (LUTD), but current methods for studying endpoints require multiple analysis techniques that contribute to an overall lengthy process. However, developments in magnetic resonance imaging (MRI) have opened the door for more accurate and time efficient methods. The purpose of this study was to demonstrate the capabilities of MRI for the analysis of LUTD in mice. To do this, whole and partial urogenital tracts were extracted from mice and imaged on a 9.4 Tesla MRI system. Additionally, a device was designed and fabricated to aid in the imaging of up to 100 mouse urogenital tracts in a single imaging session. Images were processed for both qualitative representation of MRI resolution capabilities and quantitative measurements of urogenital tract components. Even the smallest anatomical structures of the urogenital tracts were resolved and quantified, including the ureters, urethra, ductus deferens, and fine nodules and textures on the seminal vesicles, bladder, and prostatic lobes. The visual representations and urogenital component quantifications demonstrated in this study may be of value in lesion detection, diagnosis, and LUTS symptom progression tracking.

Keywords: MRI, lower urinary tract dysfunction, BPH, urogenital

Introduction

As the general population ages in the United States, incidence of benign prostatic hyperplasia (BPH) increases. BPH is a disease that develops as a consequence of aging and affects 90% of men over the age of 80 [3]. Along with the development of BPH, many men can also develop lower urinary tract symptoms (LUTS), which significantly decrease quality of life. While BPH is not a malignant disease, the development of LUTS can lead to increased frequency of urination, nocturia, and severe complications such as bladder stones and renal failure [9, 10]. Typically, BPH is characterized by the enlargement of the prostate and is diagnosed using the AUA symptom index (AUASI) score, uroflowmetry, prostate-specific antigen (PSA) blood tests, and measurement of prostate size [4, 10].

The human prostate consists of three distinct histological zones: central, peripheral, and transition [6]. Prostate cancer primarily develops in the peripheral zone, while BPH is almost exclusively found in the transition zone. The transition zone of the prostate surrounds the urethra; therefore, enlargement of the prostate can result in urethral narrowing as the prostate pushes inward due to encapsulation [1]. This urethral narrowing can lead to bladder outlet obstruction (BOO) and directly contributes to the development of LUTS. To study this, hormone-induced models of lower urinary tract dysfunction (LUTD) have been used in mice [7]. The hormone treatment leads to increased bladder size, decreased uroflow, and even kidney failure, closely mimicking BPH/LUTS in humans [4, 7]. While this model has been essential in characterizing some of the underlying macro mechanisms of BPH, the process of

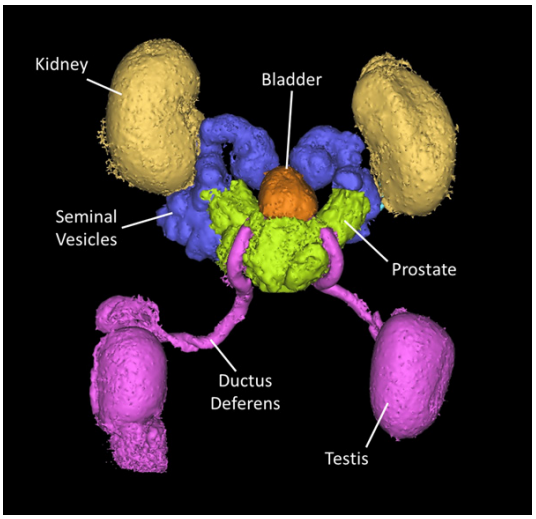

Figure 1. MRI of Adult Mouse Urogenital Tract: A full urogenital tract was dissected from an adult C57BL/6 mouse and embedded into agar gel for imaging. Following imaging, MIMICS was used to segment the different regions and tissues of the tract.

analyzing some of the more nuanced mechanisms remains tedious and time consuming. Even though the anatomy of the mouse prostate differs from that of humans, LUTD and decreased uroflow in these mice could be attributed to mechanisms that are pathologically relevant in humans as well. These mechanisms include collagen deposition, increased duct number, hyperplasia, and overall decreased urethral volume [2, 8, 13].

Current methods for analyzing BPH-related end points in mice rely on a number of steps including harvesting the urethra from the mouse after sacrifice, embedding the urethra, sectioning the urethra, and staining urethral tissue with hematoxylin and eosin. In order to reconstruct these urethras in three dimensions and measure total luminal volume, it is necessary to use hundreds of sections from a 2-3 mm portion of prostatic urethra. After staining, each urethral section is imaged, traced, and reconstructed usinga 3D reconstruction software. This process can take up to a week per mouse. If researchers aim to reconstruct tracts, including prostatic ducts and surrounding structures, it can take up to a year. In this report, we describe a magnetic resonance imaging (MRI) technique that allows for imaging and processing of urogenital tracts of mice at a very high resolution. In addition, measurements of the resulting MRI images are equal to, or outnumber, what can be reasonably measured in reconstructed tracts using previously established software, all within a fraction of the time. Finally, this MRI technique may be clinically valuable in BPH diagnosis-a process which often uses questionnaires and a digital rectal exam that can miss the underlying causes that can vary from patient to patient [12].

Material and methods

Preparation of tissues

An entire urogenital tract from an untreated C57BL/6 mouse was harvested, as previously described [7]. The entire urogenital tract below the kidneys was harvested, including the ureters, urethra, ductus deferens, seminal vesicles, bladder, and prostatic lobes. Additionally, five other mouse urogenital tracts, including the bladder and urethra, were extracted for imaging. To prevent motion of the tracts during the imaging process, they were embedded into 0.7% agar/PBS gel in 5 mL Eppendorf tubes. Agar was also used to preserve protein in the tracts so that further analysis could be conducted following imaging. After imaging was completed, the agar was rinsed off of the tracts using de-ionized water and then either transferred back to 70% EtOH for preservation or paraffin embedded for later sectioning and staining.

Holding device for large quantities of urethras

To image larger quantities of mouse urethra tissues (more than just 5) in a single imaging session, a holding device was designed. The device, shown in **Figure 3**, consists of 10 stacked disks, each with 10 open slots for housing mouse urethra segments (100 total slots). The disk (**Figure 3A**) diameter was designed to fit inside the magnet bore, and each slot has a height of 4 mm, a width of 15 mm, and a depth of 4 mm. In an effort to reduce MR image artifact, a hemispherical segment was added to each end of the device to reduce susceptibility, as shown in **Figure 3B**. The urethra holder was fabricated with a stereolithography additive manufacturing machine (Form 2, Formlabs, Somerville, MA). The resulting device is shown in **Figure 3C**. This “stackable urethra MRI organizer capsule” was termed the *SUMO-cap*.

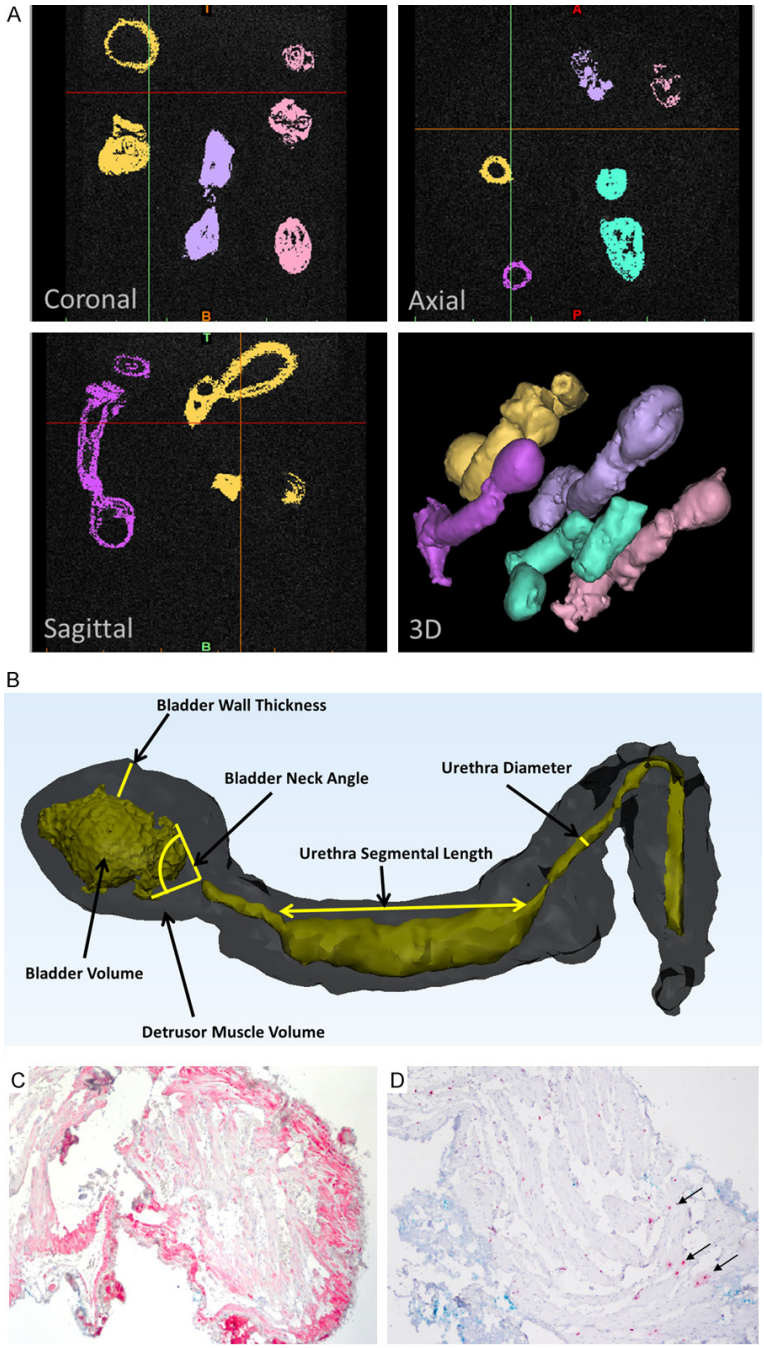

Figure 2. MRI Imaging of Mouse Bladders and Urethras: (A) Five mouse bladders and urethras were dissected and embedded into agar gel for MR imaging. Imaging produced views of the lumens of the bladders and urethras in coronal, axial, or sagittal views. These were used for subsequent measurement. (B) An example of one of the embedded tracts with selected endpoints for measurement. All measurements of the 5 tracts are included in **Table 1**. (C) Immunohistochemistry for SMA was performed to demonstrate protein preservation in the agar. (D) A BrdU stain of the selected mouse urethra demonstrating protein preservation.

To test the utility of the SUMO-cap, 69 prostatic urethras were extracted from mice and embedded into 7 of the SUMO-cap disks. Using the 9.4T MRI machine, the capsule was scanned with the same imaging protocol as the previous mouse tract imaging. Images were then imported into MIMICS and 2D and 3D views were constructed to allow for quick volume measurements.

MRI imaging protocol

The prepared samples were imaged in a 9.4T animal MRI scanner (Bruker, Billerica, MA), using a dedicated coil. MR imaging was performed using a high-resolution 3D rapid acquisition with resolution enhancement (RARE) technique including inversion recovery to approximately null the signal from agar. Imaging parameters included the following: repetition time (TR): 4000 ms, inversion time (TI): 1346 ms, echo time (TE): 55.4 ms, echo train length (ETL): 16, pixel bandwidth: 312.5 Hz, acquisition matrix: 320×320×280, spatial resolution: 0.1×0.1×0.1 mm^3.

Measurement and reconstruction of selected endpoints

The MR images, containing data from the entire untreated C57BL/6 mouse urogenital tract and from the 5 mouse urogenital tracts, were imported into MIMICS (Materialise, Leuven, Belgium) and 3-matic (Materialise, Leuven, Belgium). Key features were measured, including maximum and minimum bladder wall thickness, detrusor muscle volume, bladder volume, bladder neck angle, urethra diameters, urethra total length, and urethra segmental lengths (as displayed in **Figure 2B**). To make these measurements, the anatomical boundaries of each uro-

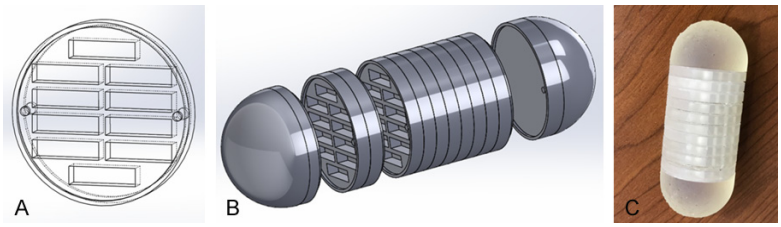

Figure 3. Design of SUMO-cap: A device was deigned to hold excised mouse urethral tracts for MR imaging. A. The device consisted of stackable disks, each with 10 slots for urethra mounting. B. Hemispherical end-caps were added to the device assembly to improve image quality by reducing susceptibility artifacts. C. The final device, consisting of 10 stacked disks, was fabricated with a stereolithography additive manufacturing methods.

genital tract were manually segmented in MIMICS based on delineation of tissue thresholds (**Figure 2**). Once each boundary was delineated, 3D models of each urogenital tract were exported to 3-matic for further processing. Maximum and minimum bladder wall thicknesses were determined by first separating the bladder wall volume from the remainder of the tract and then computing the maximum and minimum wall thickness points in 3-matic. Bladder and detrusor muscle volumes were calculated by first subtracting the 3D bladder fluid volume from the bladder wall and then calculating the volume of each by totaling the number of voxels in each part. Bladder neck angle was determined by finding the mean tangent points between the urethra opening and the bladder wall on opposing sides of the bladder, as shown in **Figure 2B**. Urethral diameters, total length, and segmental lengths were found by segmenting the urethral opening and then measuring at various points on the 3D segmented model.

Results

MRI of full-length urogenital tract

MR images of the entire C57BL/6 untreated mouse urogenital tract were reconstructed in three dimensions with high detail (**Figure 1**). Despite a high field of view and a large amount of tissue volume, measurements were successfully conducted on even the smallest anatomical structures, including the ureter volumes, urethra volumes, and ductus deferens. Due to the high resolution of the images, fine textures and nodules of the seminal vesicles, bladder, and prostatic lobes were observed. This may be an important factor in studies that focus on lesion or nodule detection in models of cancer or BPH.

T MRI of mouse urogenital tracts and preservation

The five male urogenital tracts were successfully imaged simultaneously at a resolution of 0.1×0.1×0.1 mm^3. This resolution was previously unachievable using standard clinical ultrasound procedure. The measurements that are most relevant to the development of BPH/LUTS or LUTD in mice are shown in **Figure 2B**. Upon completion, tracts were removed from agar and embedded. Preservation of protein within the tissue was demonstrated through staining of the tracts with smooth muscle actin (SMA) and BrdU, as shown in **Figure 2C** and **2D**.

Measurements of selected endpoints

Urethral narrowing, increased bladder size, thickening of detrusor muscle, and smooth muscle changes in a T + E_2 model of LUTD were previously reported [7]. In this study, minimum and maximum bladder wall thickness were reported, which were measurements done qualitatively in the past. A summary of tract measurements is shown in **Table 1**. Bladder wall thicknesses ranged from 0.19 mm to 2.1 mm. Additionally, detrusor muscle volume in these samples ranged from 40.5 mm^3 to 95.58 mm^3. Bladder volumes of these mice ranged from 2.53 mm^3 to 67.53 mm^3. Bladder neck angle varied from 65.99° to 93.46° (**Table 1**). Finally, urethral lengths and diameters ranged from 0.85 mm to 1.87 mm.

Imaging of large quantities of urethras using SUMO-cap

The SUMO-cap was successfully imaged with 69 urethra tissue samples. The results were visualized in MIMICS, as shown in **Figure 4**. Although imaging of the SUMO-cap was performed to demonstrate usefulness of the device, the individual urethra dimensions could be quantified, as was done on the 5 male mouse urogenital tracts earlier in this work.

Discussion

In this study, an improved technique to characterize and investigate LUTD in mice was established. Using a 9.4T MRI, a spatial resolution of

Table 1. Selected endpoint measurements of full length urogenital tracts

Mouse	Bladder Wall Thickness (Max) (mm)	Bladder Wall Thickness (Min)	Detrusor Muscle Volume (mm^3)	Bladder Volume (mm^3)	Bladder Neck Angle (degrees)	Urethra length (mm)	Urethra Diameter (mm)
1	1.7	0.19	44.99	13.29	76.79	21.76	1.48
2	1.47	0.3	49.02	67.53	93.46	22.11	1.87
3	2.1	0.47	95.58	22.79	67.13	21.91	1.03
4	1.54	0.51	43.57	12.32	71.91	25.57	1.02
5	1.65	0.91	40.5	2.53	65.99	22	0.85

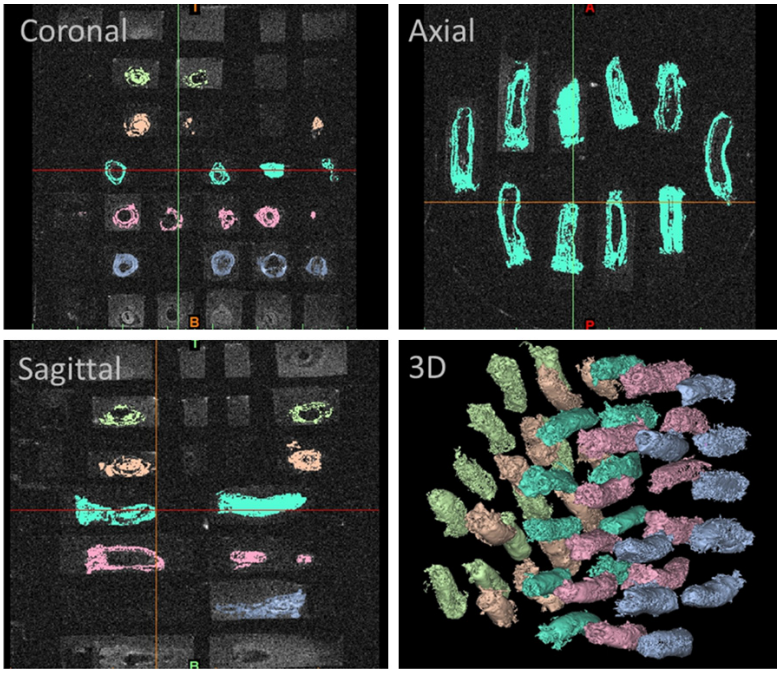

Figure 4. MRI Imaging in High Density SUMO-cap: 69 Adult mouse prostatic urethras were embedded in agar gel in the SUMO-cap and imaged under the same MRI protocol as previously described. All 69 urethras were visualized in a 3D space, and 2D views allowed clear visualization of urethral lumens for subsequent measurement.

$0.1\times0.1\times0.1$ mm^3 was achieved. In the clinic, men with BPH often present with LUTS and enlargement of the prostate. Researchers have shown that this can lead to increased bladder size, increased frequency of urination, and nocturia [11]. This can be attributed to a number of causes, including changes in bladder neck angle, which is caused by the prostate pushing up against the bladder. This changes uroflow dynamics and causes incomplete voiding [5]. LUTS can also be attributed to BOO, which is most often caused by prostate enlargement resulting in urethral narrowing [11]. In this mouse model, which is at a much smaller scale than previous studies, reliable measurement accuracy was shown on multiple endpoints. Additionally, several tracts were reconstructed and measured using a single imaging session, which provides results in a fraction of the time as is required by current techniques. These measurements also allow for characterization of obstruction and for follow-up histological studies to determine the cause of the obstruction (such as increased fibrosis or smooth muscle). Past methods of analysis have relied on sectioning and staining the entire urethra to determine the cause of obstruction. LUTS or BOO, leading to urinary retention, is often very hard to predict and can have variable causes between patients. With this MRI protocol, causes of BPH/LUTS can be found in mouse models with improved accuracy over established methods, such as ultrasound. Future studies will focus on using this protocol to interrogate causes of BPH/LUTS, such as hormonal changes. Additionally, this protocol can be optimized for imaging of live mice, which would allow for longitudinal studies and monitoring of physiological changes following standard and novel treatments.

Acknowledgements

We would like to acknowledge funding from the following sources: T32 CA009135 (DTM), R01 ES001332 (WAR), U54 DK104310, and UWCCC P30CA014520.

Disclosure of conflict of interest

None.

Address correspondence to: Alejandro Roldán-Alzate, Mechanical Engineering, University of Wisconsin, 1513 University Avenue, Room ME 3035, Madison, WI 53705, USA. Tel: (608) 262-1780; E-mail: roldan@wisc.edu

References

[1] Aaron L, Franco OE, Hayward SW. Review of prostate anatomy and embryology and the etiology of benign prostatic hyperplasia. Urol Clin North Am 2016; 43: 279-88.

[2] Bauman TM, Nicholson TM, Abler LL, Eliceiri KW, Huang W, Vezina CM, Ricke WA. Characterization of fibrillar collagens and extracellular matrix of glandular benign prostatic hyperplasia nodules. PLoS One 2014; 9: e109102.

[3] Berry SJ, Coffey DS, Walsh PC, Ewing LL. The development of human benign prostatic hyperplasia with age. J Urol 1984; 132: 474-479.

[4] Egan KB. The epidemiology of benign prostatic hyperplasia associated with lower urinary tract symptoms: prevalence and incident rates. Urol Clin North Am 2016; 43: 289-97.

[5] Mangera A, Osman NI, Chapple CR. Assessment of BPH/BOO. Indian J Urol 2014; 30: 177-80.

[6] McNeal JE. Origin and evolution of benign prostatic enlargement. Invest Urol 1978; 15: 340-5.

[7] Nicholson TM, Ricke EA, Marker PC, Miano JM, Mayer RD, Timms BG, vom Saal FS, Wood RW, Ricke WA. Testosterone and 17beta-estradiol induce glandular prostatic growth, bladder outlet obstruction, and voiding dysfunction in male mice. Endocrinology 2012; 153: 5556-65.

[8] Nicholson TM, Ricke WA. Androgens and estrogens in benign prostatic hyperplasia: past, present and future. Differentiation 2011; 82: 184-99.

[9] Oelke M, Kirschner-Hermanns R, Thiruchelvam N, Heesakkers J. Can we identify men who will have complications from benign prostatic obstruction (BPO)? ICI-RS 2011. Neurourol Urodyn 2012; 31: 322-6.

[10] Roehrborn CG. Benign prostatic hyperplasia: an overview. Rev Urol 2005; Suppl 9: S3-S14.

[11] Roehrborn CG. Male lower urinary tract symptoms (LUTS) and benign prostatic hyperplasia (BPH). Med Clin North Am 2011; 95: 87-100.

[12] Tanguay S, Awde M, Brock G, Casey R, Kozak J, Lee J, Nickel JC, Saad F. Diagnosis and management of benign prostatic hyperplasia in primary care. Can Urol Assoc J 2009; Suppl 2: S92-S100.

[13] Trumbeckas D, Milonas D, Jievaltas M, Matjosaitis AJ, Kincius M, Grybas A, Kopustinskas V. Importance of prostate volume and urinary flow rate in prediction of bladder outlet obstruction in men with symptomatic benign prostatic hyperplasia. Cent European J Urol 2011; 64: 75-9.